Fourier Transform Sound Radiation

F. X. Xin and T. J. Lu

State Key Laboratory for Mechanical Structure Strength and Vibration, School of Aerospace, Xi'an Jiaotong University, Xi'an,

China

1. Introduction

With the increasing use of periodically rib-stiffened composite sandwich structures as the cabin skin of aircrafts, marine ships and express trains etc. [1-5], great efforts have been made in the pursuit of efficient theoretical methods for predicting the vibration and acoustic behaviors of these lightweight structures, so as to design optimized configurations competent for practical low-noise requirements.

Active control algorithms with sensors and actuators have been developed to reduce structural vibration and sound radiation [6], which however inevitably brings the penalty of increasing system complexity and financial costs. Alternatively, passive measures such as inserting fibrous sound absorptive materials in the partitioned cavity of sandwich structures may be a preferable choice to achieve a compromise between noise-reduction efficiency and financial cost. For instance, the fuselages of commercial aircrafts are commonly made of periodically rib-stiffened composite structures filled with fiberglass to enhance thermal and sound insulation [6-9]. This provides strong impetus for the development of effective theoretical models to predict the sound radiation characteristics of periodically rib-stiffened sandwich structures filled with sound absorptive materials.

There exist numerous theoretical models for the vibroacoustic behaviors of periodic ribstiffened structures, which may be grouped into two main categorizes: one is based on the Fourier transform method [2-4,10-13], which is able to handle both sound radiation and sound transmission problems; the other is built upon the space-harmonic approach [14-18], which are suited particularly for sound transmission problems. Mace [2] employed the Fourier transform method to solve the problem of sound radiation from a fluid-loaded infinite plate reinforced by two sets of parallel stiffeners when excited by a point force; for simplification, only the tensional force of the rib-stiffeners was considered. Subsequently, Mace [3] proposed a theoretical model for the radiation of sound from an infinite fluid loaded plate when the plate is reinforced with two sets of orthogonal line stiffeners; again, only the tensional force of the rib-stiffeners was accounted for. Similarly, by only taking account of the normal force interaction between panel and rib-stiffeners, Yin et al. [4] presented a simplified theoretical model for acoustic radiation from a point-driven, fluidloaded infinite laminated composite plate reinforced by periodic parallel rib-stiffeners.

As an essentially equivalent method, the space-harmonic approach evolved from progressive wave propagation was initiated by Mead and Pujara [14] when they studied the acoustical response of periodical stiffened beams subjected to a spatial and temporal harmonic pressure. It was demonstrated that as few as three terms of space harmonics could lead to solutions of acceptable accuracy. By combining the space-harmonic approach and virtual energy method, Lee and Kim [15] analyzed the sound transmission characteristics of a thin plate stiffened by equally spaced line stiffeners. By modeling the rib-stiffeners as a combination of translational springs and rotational springs, Wang et al. [16] proposed an analytical model for sound transmission loss across double-leaf partitions stiffened with periodically placed studs. Recently, Xin and Lu [18] developed a comprehensive analytical model for sound transmission through orthogonally rib-stiffened sandwich structures: all possible motions of the rib-stiffeners were accounted for by introducing the tensional forces, bending moments and torsional moments as well as the corresponding inertial terms into the governing equations of the two face panels.

None of the above mentioned investigations dealt with sound radiation and/or sound transmission issues of composite sandwich structures filled with porous sound absorptive materials. As far as the sound radiation/transmission problems of double partitions with cavity absorption is of concern, a number of theoretical [12,13], numerical [19,20] and experimental [21] studies do exist. However, all of these studies did not consider the effects of structural rib-connections between two face panels, which may be far away from the factual engineering structures. To address this deficiency, a comprehensive theoretical model is developed here for the radiation of sound from an infinite orthogonally ribstiffened sandwich structure filled with fibrous sound absorptive material in the partitioned cavity when excited by a time-harmonic point force. The equivalent forces and moments (both bending and torsional) imposed on the two face panels by the rib-stiffeners are accounted for by considering all possible motions of the rib-stiffeners. By employing the well-known equivalent fluid model [12,22], wave propagation in the fibrous sound absorptive material can be accurately described. Both viscous drag forces and thermal exchanges between air and solid fibers are accounted for by introducing frequency dependent dynamic density and bulk modulus. Taking advantage of the periodical property of the composite sandwich structure, the Fourier transform technique is adopted to solve both the structural and acoustical governing equations. In limiting cases the developed model can be favorably degraded to deal with sound radiation issues of sandwich structures with vacuum or air cavities. Therefore, model validation is carried out by comparing the present predictions for simplified sandwich structures with those available in the open literature. To explore the influence of fibrous sound absorptive materials on sound radiation of orthogonally rib-stiffened composite structures, numerical results are presented, with relevant physical features interpreted in detail. Conclusions drawn from the present theoretical study may provide fundamental principles for factual engineering design of ribstiffened composite structures filled with fibrous sound absorptive materials.

2. Structural dynamic responses to time-harmonic point force

2.1 Analytical formulation of panel vibration

Consider an infinite sandwich structure as shown schematically in Fig. 1, which is reinforced by two periodic sets of orthogonal rib-stiffeners having periodic uniform separations l_x and l_y in the x- and y-directions, respectively. A right-handed Cartesian coordinate system (x, y, z) is established, with its x-axis and y-axis positioned separately

along one pair of the orthogonal rib-stiffeners, the positive direction of the z-axis pointing downward (Fig. 1). Three different kinds of sandwich structures will be considered in the proceeding sections, namely, the gap between the two parallel face panels and portioned by the orthogonal lattice cores is in vacuum, air filled, or filled with fibrous sound absorptive material (e.g., fiberglass), respectively. A theoretical model will be formulated for the complex structure (i.e., orthogonally rib-stiffened sandwich structure filled with fibrous sound absorptive material), which can be degraded to deal with the other two sandwiches.

Assume that a time-harmonic point force $q_0e^{i\omega t}$ acts on the surface of the upper panel at location (x_0,y_0) ; see Fig. 1. Consequently, a radially outspreading bending wave propagates in the upper panel from the source (x_0,y_0) . The vibration of the upper panel is transmitted to the bottom panel via the orthogonal rib-stiffeners and sound-absorbing material (or air cavity). Subsequently, the bottom panel vibrates and radiates sound pressure waves.

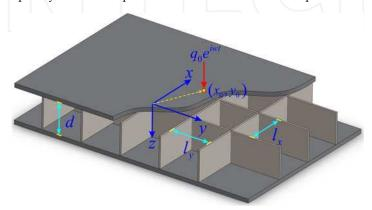


Fig. 1. Schematic illustration of orthogonally rib-stiffened sandwich structure (three different kinds: vacuum cavity, air cavity, and fiberglass filled cavity) excited by time-harmonic point force at (x_0, y_0)

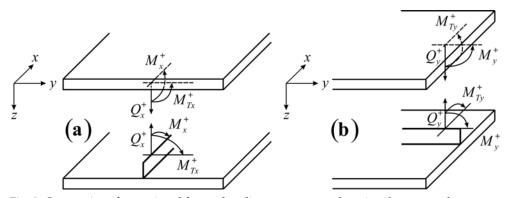


Fig. 2. Conventions for tensional forces, bending moments and torsional moments between upper panel and (a) x-wise and (b) y-wise stiffeners, which also hold at the interface between bottom panel and x- and y-wise stiffeners

Upon point force excitation, the vibration of the upper and bottom panels can be described using two dynamic governing equations, where the influence of the rib-stiffeners exists in the form of tensional forces (general force plus inertial force), bending moments (general bending moment plus inertial bending moment), and torsional moments (general torsional moment plus inertial torsional moment). With the inertial effects of the rib-stiffeners accounted for, the resultant tensional forces, bending and torsional moments acting on the upper and bottom panels per rib-stiffener are not equal, denoted here by (Q^+, M^+, M_T^+) and (Q^-, M^-, M_T^-) , respectively. Fig. 2 shows the convention employed for denoting the tensional forces as well as the bending and torsional moments between the upper panel and the x- and y-wise stiffeners. The same apply at the interface between the bottom panel and the x- and y-wise stiffeners.

The dynamic responses of the sandwich structure are time-harmonic as the excitation is in the form of $q_0e^{i\omega t}$. For simplicity, the harmonic time term $e^{i\omega t}$ is suppressed henceforth. With the equivalent forces and moments of the lattice core and the pressure in the fibrous sound absorptive material (or air cavity) accounted for, the equations governing panel vibrations are given by:

$$D_{1}\nabla^{4}w_{1} + m_{1}\frac{\partial^{2}w_{1}}{\partial t^{2}} = \sum_{m=-\infty}^{+\infty} \left[Q_{y}^{+}\delta(x - ml_{x}) + \frac{\partial}{\partial y} \left\{ M_{y}^{+}\delta(x - ml_{x}) \right\} + \frac{\partial}{\partial x} \left\{ M_{Ty}^{+}\delta(x - ml_{x}) \right\} \right]$$

$$+ \sum_{n=-\infty}^{+\infty} \left[Q_{x}^{+}\delta(y - nl_{y}) + \frac{\partial}{\partial x} \left\{ M_{x}^{+}\delta(y - nl_{y}) \right\} + \frac{\partial}{\partial y} \left\{ M_{Tx}^{+}\delta(y - nl_{y}) \right\} \right]$$

$$+ q_{0}\delta(x - x_{0})\delta(y - y_{0}) - p_{cav}(x, y, h_{1})$$

$$(1)$$

$$D_{2}\nabla^{4}w_{2} + m_{2}\frac{\partial^{2}w_{2}}{\partial t^{2}} = -\sum_{m=-\infty}^{+\infty} \left[Q_{y}^{-}\delta(x - ml_{x}) + \frac{\partial}{\partial y} \left\{ M_{y}^{-}\delta(x - ml_{x}) \right\} + \frac{\partial}{\partial x} \left\{ M_{Ty}^{-}\delta(x - ml_{x}) \right\} \right]$$

$$-\sum_{n=-\infty}^{+\infty} \left[Q_{x}^{-}\delta(y - nl_{y}) + \frac{\partial}{\partial x} \left\{ M_{x}^{-}\delta(y - nl_{y}) \right\} + \frac{\partial}{\partial y} \left\{ M_{Tx}^{-}\delta(y - nl_{y}) \right\} \right]$$

$$+ p_{can}(x, y, h_{1} + d)$$

$$(2)$$

where $\nabla^4 \equiv \left(\frac{\partial^2}{\partial x^2} + \frac{\partial^2}{\partial y^2} \right)^2$; $\delta(\cdot)$ is the Dirac delta function; (w_1, w_2) , (m_1, m_2) and (D_1, D_2) are the displacement, surface mass density and flexural rigidity of the upper panel and bottom panel, respectively. The material loss factor η_j (j = 1, 2 for upper panel and bottom panel, respectively) is introduced with the complex Young's modulus $D_j = E_j h_j^3 \left(1 + i \eta_j\right) / 12 \left(1 - v_j^2\right)$ (where j = 1, 2).

As the factual forces and moments exerting on the upper and bottom panels are not the same due to the consideration of inertial forces and moments, the terms associated with the two panels are denoted separately by superscripts + (upper) and – (bottom). Subscripts x and y are introduced to represent those terms arising from the x- and y-wise stiffeners, respectively.

Taking into account the inertial effects (due to stiffener mass) and applying both the Hooke's law and Newton's second law, one obtains the tensional forces arising from the rib-stiffeners as [18]:

$$Q_x^+ = -\frac{K_x \left(K_x - m_x \omega^2\right)}{2K_x - m_x \omega^2} w_1 + \frac{K_x^2}{2K_x - m_x \omega^2} w_2 \tag{3}$$

$$Q_{x}^{-} = -\frac{K_{x}^{2}}{2K_{x} - m_{x}\omega^{2}}w_{1} + \frac{K_{x}(K_{x} - m_{x}\omega^{2})}{2K_{x} - m_{x}\omega^{2}}w_{2}$$
(4)

$$Q_{y}^{+} = -\frac{K_{y}(K_{y} - m_{y}\omega^{2})}{2K_{y} - m_{y}\omega^{2}}w_{1} + \frac{K_{y}^{2}}{2K_{y} - m_{y}\omega^{2}}w_{2}$$
(5)

$$Q_{y}^{-} = -\frac{K_{y}^{2}}{2K_{y} - m_{y}\omega^{2}}w_{1} + \frac{K_{y}(K_{y} - m_{y}\omega^{2})}{2K_{y} - m_{y}\omega^{2}}w_{2}$$
 (6)

where ω is the circle frequency and (K_x, K_y) are the tensional stiffness of half the rib-stiffeners per unit length.

Similarly, the bending moments of the rib-stiffeners can be expressed as [18]:

$$M_{x}^{+} = \frac{E_{x}I_{x}^{*} \left(E_{x}I_{x}^{*} - \rho_{x}I_{x}\omega^{2}\right)}{2E_{x}I_{x}^{*} - \rho_{x}I_{x}\omega^{2}} \frac{\partial^{2}w_{1}}{\partial x^{2}} - \frac{E_{x}^{2}I_{x}^{*2}}{2E_{x}I_{x}^{*} - \rho_{x}I_{x}\omega^{2}} \frac{\partial^{2}w_{2}}{\partial x^{2}}$$
(7)

$$M_{x}^{-} = \frac{E_{x}^{2} I_{x}^{*2}}{2E_{x} I_{x}^{*} - \rho_{x} I_{x} \omega^{2}} \frac{\partial^{2} w_{1}}{\partial x^{2}} - \frac{E_{x} I_{x}^{*} \left(E_{x} I_{x}^{*} - \rho_{x} I_{x} \omega^{2}\right)}{2E_{x} I_{x}^{*} - \rho_{x} I_{x} \omega^{2}} \frac{\partial^{2} w_{2}}{\partial x^{2}}$$
(8)

$$M_{y}^{+} = \frac{E_{y}I_{y}^{*} \left(E_{y}I_{y}^{*} - \rho_{y}I_{y}\omega^{2}\right)}{2E_{y}I_{y}^{*} - \rho_{y}I_{y}\omega^{2}} \frac{\partial^{2}w_{1}}{\partial y^{2}} - \frac{E_{y}^{2}I_{y}^{*2}}{2E_{y}I_{y}^{*} - \rho_{y}I_{y}\omega^{2}} \frac{\partial^{2}w_{2}}{\partial y^{2}}$$
(9)

$$M_{y}^{-} = \frac{E_{y}^{2} I_{y}^{*2}}{2E_{y} I_{y}^{*} - \rho_{y} I_{y} \omega^{2}} \frac{\partial^{2} w_{1}}{\partial y^{2}} - \frac{E_{y}^{2} I_{y}^{*} \left(E_{y} I_{y}^{*} - \rho_{y} I_{y} \omega^{2}\right)}{2E_{y} I_{y}^{*} - \rho_{y} I_{y} \omega^{2}} \frac{\partial^{2} w_{2}}{\partial y^{2}}$$
(10)

where $(E_x I_x^*, E_y I_y^*)$ are the bending stiffness of half the rib-stiffeners, (ρ_x, ρ_y) and (I_x, I_y) are mass density and polar moment of inertia for the rib-stiffeners, with subscripts x and y indicating the direction of the stiffener.

Following similar procedures for deriving the tensional forces and bending moments, one obtains the torsional moments of the rib-stiffeners as [18]:

$$M_{Tx}^{+} = \frac{G_x J_x^{*} \left(G_x J_x^{*} - \rho_x J_x \omega^2\right)}{2G_x J_x^{*} - \rho_x J_x \omega^2} \frac{\partial^2 w_1}{\partial x \partial y} - \frac{G_x^2 J_x^{*2}}{2G_x J_x^{*} - \rho_x J_x \omega^2} \frac{\partial^2 w_2}{\partial x \partial y}$$
(11)

$$M_{Tx}^{-} = \frac{G_x^2 J_x^{*2}}{2G_x J_x^{*} - \rho_x J_x \omega^2} \frac{\partial^2 w_1}{\partial x \partial y} - \frac{G_x J_x^{*} \left(G_x J_x^{*} - \rho_x J_x \omega^2\right)}{2G_x J_x^{*} - \rho_x J_x \omega^2} \frac{\partial^2 w_2}{\partial x \partial y}$$
(12)

$$M_{Ty}^{+} = \frac{G_{y}J_{y}^{*} \left(G_{y}J_{y}^{*} - \rho_{y}J_{y}\omega^{2}\right)}{2G_{y}J_{y}^{*} - \rho_{y}J_{y}\omega^{2}} \frac{\partial^{2}w_{1}}{\partial y\partial x} - \frac{G_{y}^{2}J_{y}^{*2}}{2G_{y}J_{y}^{*} - \rho_{y}J_{y}\omega^{2}} \frac{\partial^{2}w_{2}}{\partial y\partial x}$$
(13)

$$M_{Ty}^{-} = \frac{G_y^2 J_y^{*2}}{2G_y J_y^* - \rho_y J_y \omega^2} \frac{\partial^2 w_1}{\partial y \partial x} - \frac{G_y J_y^* \left(G_y J_y^* - \rho_y J_y \omega^2\right)}{2G_y J_y^* - \rho_y J_y \omega^2} \frac{\partial^2 w_2}{\partial y \partial x}$$
(14)

where $(G_xJ_x^*, G_yJ_y^*)$ are the torsional stiffness of half the rib-stiffeners and (J_x, J_y) are the torsional moment of inertia for the rib-stiffeners.

In the above expressions for the tensional forces, bending moments and torsional moments of a rib-stiffener, the geometrical properties of its cross-section are given by:

$$K_x = \frac{E_x t_x}{d/2}, K_y = \frac{E_y t_y}{d/2}$$
 (15)

$$I_x^* = \frac{t_x (d/2)^3}{12}$$
, $I_y^* = \frac{t_y (d/2)^3}{12}$, $I_x = \frac{t_x d^3}{12}$, $I_y = \frac{t_y d^3}{12}$ (16)

$$J_x^* = \frac{t_x^3 d}{2} \left[\frac{1}{3} - \frac{64}{\pi^5} \frac{2t_x}{d} \sum_{n=1,3,5,\dots}^{\infty} \frac{\tanh(n\pi d / 4t_x)}{n^5} \right]$$
 (17)

$$J_y^* = \frac{t_y^3 d}{2} \left[\frac{1}{3} - \frac{64}{\pi^5} \frac{2t_y}{d} \sum_{n=1,3,5,\dots}^{\infty} \frac{\tanh(n\pi d / 4t_y)}{n^5} \right]$$
 (18)

$$J_x = t_x^3 d \left[\frac{1}{3} - \frac{64}{\pi^5} \frac{t_x}{d} \sum_{n=1,3,5,\dots}^{\infty} \frac{\tanh(n\pi d / 2t_x)}{n^5} \right]$$
 (19)

$$J_y = t_y^3 d \left[\frac{1}{3} - \frac{64}{\pi^5} \frac{t_y}{d} \sum_{n=1,3,5}^{\infty} \frac{\tanh(n\pi d / 2t_y)}{n^5} \right]$$
 (20)

where E_x and E_y are separately the Young's modulus of the x- and y-wise stiffener materials.

To simplify Eqs. (3)-(14), the following set of specified characteristics is introduced to replace the coefficients of general displacements.

Replacement of tensional force coefficients:

$$R_{Q1} = \frac{K_x \left(K_x - m_x \omega^2 \right)}{2K_x - m_x \omega^2} , \ R_{Q2} = \frac{K_x^2}{2K_x - m_x \omega^2}$$
 (21)

$$R_{Q3} = \frac{K_y \left(K_y - m_y \omega^2 \right)}{2K_y - m_y \omega^2}, \ R_{Q4} = \frac{K_y^2}{2K_y - m_y \omega^2}$$
 (22)

2. Replacement of bending moment coefficients:

$$R_{M1} = \frac{E_x I_x^* \left(E_x I_x^* - \rho_x I_x \omega^2 \right)}{2E_x I_x^* - \rho_x I_x \omega^2}, \ R_{M2} = \frac{E_x^2 I_x^{*2}}{2E_x I_x^* - \rho_x I_x \omega^2}$$
(23)

$$R_{M3} = \frac{E_y I_y^* \left(E_y I_y^* - \rho_y I_y \omega^2 \right)}{2E_\nu I_y^* - \rho_\nu I_y \omega^2}, \ R_{M4} = \frac{E_y^2 I_y^{*2}}{2E_\nu I_y^* - \rho_\nu I_y \omega^2}, \tag{24}$$

3. Replacement of torsional moment coefficients:

$$R_{T1} = \frac{G_x J_x^* \left(G_x J_x^* - \rho_x J_x \omega^2 \right)}{2G_x J_x^* - \rho_x J_x \omega^2}, \ R_{T2} = \frac{G_x^2 J_x^{*2}}{2G_x J_x^* - \rho_x J_x \omega^2},$$
 (25)

$$R_{T3} = \frac{G_y J_y^* \left(G_y J_y^* - \rho_y J_y \omega^2 \right)}{2G_y J_y^* - \rho_y J_y \omega^2}, \ R_{T4} = \frac{G_y^2 J_y^{*2}}{2G_y J_y^* - \rho_y J_y \omega^2}, \tag{26}$$

Using Eqs. (21)-(26), one can simplify the expressions of the tensional forces, bending moments and torsional moments, as:

1. Tensional forces

$$Q_x^+ = -R_{Q1}w_1 + R_{Q2}w_2, \ Q_x^- = -R_{Q2}w_1 + R_{Q1}w_2$$
 (27)

$$Q_y^+ = -R_{Q3}w_1 + R_{Q4}w_2, \ Q_y^- = -R_{Q4}w_1 + R_{Q3}w_2$$
 (28)

2. Bending moments

$$M_x^+ = R_{M1} \frac{\partial^2 w_1}{\partial x^2} - R_{M2} \frac{\partial^2 w_2}{\partial x^2}, M_x^- = R_{M2} \frac{\partial^2 w_1}{\partial x^2} - R_{M1} \frac{\partial^2 w_2}{\partial x^2},$$
 (29)

$$M_y^+ = R_{M3} \frac{\partial^2 w_1}{\partial y^2} - R_{M4} \frac{\partial^2 w_2}{\partial y^2}, M_y^- = R_{M4} \frac{\partial^2 w_1}{\partial y^2} - R_{M3} \frac{\partial^2 w_2}{\partial y^2},$$
 (30)

3. Torsional moments

$$M_{Tx}^{+} = R_{T1} \frac{\partial^{2} w_{1}}{\partial x \partial y} - R_{T2} \frac{\partial^{2} w_{2}}{\partial x \partial y}, \quad M_{Tx}^{-} = R_{T2} \frac{\partial^{2} w_{1}}{\partial x \partial y} - R_{T1} \frac{\partial^{2} w_{2}}{\partial x \partial y}, \tag{31}$$

$$M_{Ty}^{+} = R_{T3} \frac{\partial^2 w_1}{\partial y \partial x} - R_{T4} \frac{\partial^2 w_2}{\partial y \partial x}, \quad M_{Ty}^{-} = R_{T4} \frac{\partial^2 w_1}{\partial y \partial x} - R_{T3} \frac{\partial^2 w_2}{\partial y \partial x}, \quad (32)$$

2.2 Solutions

Given the 2D (two-dimensional) periodic nature of the sandwich structure as shown in Fig. 1, applying the Poisson summation formula [3,23], the wave components in the structure can be expressed by using space harmonic series, as:

$$\sum_{m=-\infty}^{+\infty} \delta(x - ml_x) = \frac{1}{l_x} \sum_{m=-\infty}^{+\infty} e^{-i(2m\pi/l_x)x} , \sum_{n=-\infty}^{+\infty} \delta(y - nl_y) = \frac{1}{l_y} \sum_{n=-\infty}^{+\infty} e^{-i(2n\pi/l_y)y}$$
(33)

The Fourier transform pair of a function with respect to (x, y) and (α, β) can be defined as:

$$w(x,y) = \int_{-\infty}^{+\infty} \int_{-\infty}^{+\infty} \tilde{w}(\alpha,\beta) \qquad e^{i(\alpha x + \beta y)} d\alpha d\beta \tag{34}$$

$$\tilde{w}(\alpha,\beta) = \left(\frac{1}{2\pi}\right)^2 \int_{-\infty}^{+\infty} \int_{-\infty}^{+\infty} w(x,y) e^{-i(\alpha x + \beta y)} dx dy \tag{35}$$

Applying the Poisson summation formula and then taking the Fourier transform of Eqs. (1) and (2), one gets:

$$\left[D_{1}\left(\alpha^{2}+\beta^{2}\right)^{2}-m_{1}\omega^{2}\right]\tilde{w}_{1}\left(\alpha,\beta\right) = \frac{1}{l_{x}}\sum_{m}\left[\tilde{Q}_{y}^{+}\left(\alpha_{m},\beta\right)+i\beta\tilde{M}_{y}^{+}\left(\alpha_{m},\beta\right)+i\alpha\tilde{M}_{Ty}^{+}\left(\alpha_{m},\beta\right)\right] + \frac{1}{l_{y}}\sum_{n}\left[\tilde{Q}_{x}^{+}\left(\alpha,\beta_{n}\right)+i\alpha\tilde{M}_{x}^{+}\left(\alpha,\beta_{n}\right)+i\beta\tilde{M}_{Tx}^{+}\left(\alpha,\beta_{n}\right)\right] + \frac{q_{0}}{\left(2\pi\right)^{2}}e^{-i(\alpha x_{0}+\beta y_{0})}-\tilde{p}_{cav}\left(\alpha,\beta,h_{1}\right)$$
(36)

$$\left[D_{2}\left(\alpha^{2}+\beta^{2}\right)^{2}-m_{2}\omega^{2}\right]\tilde{w}_{2}(\alpha,\beta)=-\frac{1}{l_{x}}\sum_{m}\left[\tilde{Q}_{y}^{-}(\alpha_{m},\beta)+i\beta\tilde{M}_{y}^{-}(\alpha_{m},\beta)+i\alpha\tilde{M}_{Ty}^{-}(\alpha_{m},\beta)\right] \\
-\frac{1}{l_{y}}\sum_{n}\left[\tilde{Q}_{x}^{-}(\alpha,\beta_{n})+i\alpha\tilde{M}_{x}^{-}(\alpha,\beta_{n})+i\beta\tilde{M}_{Tx}^{-}(\alpha,\beta_{n})\right]+\tilde{p}_{cav}(\alpha,\beta,h_{1}+d)$$
(37)

where $\alpha_m = \alpha + 2m\pi/l_x$, $\beta_n = \beta + 2n\pi/l_y$, and the dependence of a term on the wavenumbers (α , β) is indicated using the hat sign \sim , meaning the corresponding Fourier transform of this term. Expressions for the Fourier transform of the tensional forces, bending and torsional moments are presented below.

Fourier transforms of tensional forces

$$\tilde{Q}_{x}^{+}(a,\beta_{n}) = -R_{Q1}\tilde{w}_{1}(a,\beta_{n}) + R_{Q2}\tilde{w}_{2}(a,\beta_{n})$$

$$\tag{38}$$

$$\tilde{Q}_{x}^{-}(a,\beta_{n}) = -R_{O2}\tilde{w}_{1}(a,\beta_{n}) + R_{O1}\tilde{w}_{2}(a,\beta_{n})$$
(39)

$$\tilde{Q}_{y}^{+}(a_{m},\beta) = -R_{Q3}\tilde{w}_{1}(a_{m},\beta) + R_{Q4}\tilde{w}_{2}(a_{m},\beta)$$
(40)

$$\tilde{Q}_{\nu}^{-}(a_{m},\beta) = -R_{O4}\tilde{w}_{1}(a_{m},\beta) + R_{O3}\tilde{w}_{2}(a_{m},\beta)$$
(41)

Fourier transforms of bending moments

$$\tilde{M}_{x}^{+}(a,\beta_{n}) = -\alpha^{2} \left[R_{M1} \tilde{w}_{1}(a,\beta_{n}) - R_{M2} \tilde{w}_{2}(a,\beta_{n}) \right]$$
(42)

$$\tilde{M}_{x}^{-}(a,\beta_{n}) = -\alpha^{2} \left[R_{M2} \tilde{w}_{1}(a,\beta_{n}) - R_{M1} \tilde{w}_{2}(a,\beta_{n}) \right]$$

$$\tag{43}$$

$$\tilde{M}_{u}^{+}(a_{m},\beta) = -\beta^{2} \left[R_{M3} \tilde{w}_{1}(a_{m},\beta) - R_{M4} \tilde{w}_{2}(a_{m},\beta) \right]$$
(44)

$$\tilde{M}_{y}^{-}(a_{m},\beta) = -\beta^{2} \left[R_{M4} \tilde{w}_{1}(a_{m},\beta) - R_{M3} \tilde{w}_{2}(a_{m},\beta) \right]$$
(45)

Fourier transforms of torsional moments

$$\tilde{M}_{Tx}^{+}(a,\beta_n) = -\alpha\beta_n \left[R_{T1}\tilde{w}_1(a,\beta_n) - R_{T2}\tilde{w}_2(a,\beta_n) \right]$$
(46)

$$\tilde{M}_{Tx}^{-}(a,\beta_n) = -\alpha\beta_n \left[R_{T2}\tilde{w}_1(a,\beta_n) - R_{T1}\tilde{w}_2(a,\beta_n) \right]$$
(47)

$$\tilde{M}_{Ty}^{+}\left(a_{m},\beta\right) = -\alpha_{m}\beta \left[R_{T3}\tilde{w}_{1}\left(a_{m},\beta\right) - R_{T4}\tilde{w}_{2}\left(a_{m},\beta\right)\right] \tag{48}$$

$$\tilde{M}_{Ty}^{-}(a_m,\beta) = -\alpha_m \beta \left[R_{T4} \tilde{w}_1(a_m,\beta) - R_{T3} \tilde{w}_2(a_m,\beta) \right]$$

$$\tag{49}$$

2.3 The acoustic pressure and fluid-structure coupling

The absorption of sound absorption by porous materials mainly arises from viscous drag forces and thermal exchange loss when sound penetrates through the material [19,24-26]. There exist numerous theoretical models to address these issues, while different models may be specialized to deal with different types of porous materials. For instance, Lu et al. proposed a model for high porosity cellular metallic foams with open cells [24,25,27,28] and another model for semi-open metal foams [26]. As for fibrous materials considered here, there are two main classes of models [19]. The first one models the fibrous material as an equivalent fluid with effective density and bulk modulus [22,29,30]: under the assumption of the solid fibers being a rigid skeleton, only one compression wave propagates in the air-saturated medium, which thereby is governed by the Helmholtz equation. The other one employs the more rigorous theory of Biot [31,32] with the elasticity of the skeleton taken into account, the solution of which often seeks help from the finite element method (FEM) and suffers from huge computational expenses.

In view of the complexity of the proposed structural vibration model and the primary focus of the present study on sound radiation of the sandwich structure as a whole, the well-developed empirical expressions (i.e., equivalent fluid model) of Allard and Champoux [22] is adopted to model the acoustic pressure in fibrous absorption materials such as glass/rock wools widely used in noise absorption engineering. In terms of scholar description, these may be defined as Newtonian fluid saturated rigid frame fibrous materials, with the frame fibers randomly distributed. Although Allard and Champoux [22] called their empirical equations as the equivalent fluid model, this model is in fact based on Johnson et al.'s two phases theory [33]. It accurately accounted for the viscous forces between fluid and solid and the physical transposition in the process of sound propagation, by adopting two variables - the dynamic density $\rho(\omega)$ and the dynamic bulk modulus $K(\omega)$ - assuming that the fibrous material is isotropic. The equivalent fluid model has been demonstrated to be capable of providing accurate predictions of sound wave propagation across fibrous sound absorptive materials, over a wide frequency range, and hence has been widely acknowledged by the acoustic community [19,24-26]. To be more precise, the equivalent

fluid model is valid for most glass/rock wools for f/R smaller than 1.0 kg⁻¹m³, where f is the frequency and R is the flow resistivity of the fibrous material [22]. Generally, the flow resistivity R of typical glass/rock wools is approximately 20000 Nm/s⁴, and hence the equivalent fluid model works well for frequencies below 20 kHz.

According to the equivalent fluid model, wave propagation in fibrous sound absorptive material (e.g., fiberglass or mineral wool) is governed by [12,13,22,34]:

$$\left(\partial^2/\partial x^2 + \partial^2/\partial y^2 + \partial^2/\partial z^2\right)p_{cav} + k_{cav}^2 p_{cav} = 0$$
(50)

where p_{cav} is the sound pressure in the fibrous material and k_{cav} is the corresponding complex wavenumber, which is related to the dynamic density $\rho(\omega)$ and dynamic bulk modulus $K(\omega)$ of the fibrous material by:

$$k_{cav} = 2\pi f \sqrt{\rho(\omega)/K(\omega)}$$
 (51)

In accordance with the complex physical phenomena taking place in the fibrous material, such as thermal exchanges between air and fibers showing a significant transition with increasing frequency (i.e., isothermal process at low frequency turning to adiabatic process at high frequency) [22], the equivalent density and bulk modulus are both dynamic. In other words, the dynamic density and dynamic bulk modulus are frequency dependent, given by [22]:

$$\rho(\omega) = \rho_0 \left[1 + \left(R/\rho_0 f \right) G_1 \left(\rho_0 f/R \right) / i2\pi \right]$$
(52)

$$K(\omega) = \gamma_{s} P_{0} \left(\gamma_{s} - \frac{\gamma_{s} - 1}{1 + \left(\frac{1}{i8\pi N_{pr}} \right) \left(\rho_{0} f / R \right)^{-1} G_{2} \left(\rho_{0} f / R \right)} \right)^{-1}$$
 (53)

where $G_1(\rho_0f/R) = \sqrt{1+i\pi(\rho_0f/R)}$, $G_2(\rho_0f/R) = G_1\big[(\rho_0f/R)4N_{\rm pr}\big]$, R is the static flow resistivity of the fibrous material, γ_s and ρ_0 are separately the specific heat ratio (i.e., $\gamma_s = c_p/c_v$, c_p and c_v being the specific heat per unit mass of the air at constant pressure and constant volume) and density of air, P_0 is the air equilibrium pressure and $N_{\rm pr}$ is the Prandtl number. As a further understanding of physical meanings, the dynamic density $\rho(\omega)$ contains the inertial and viscous forces per unit volume of air in fibrous material, while the dynamic bulk modulus $K(\omega)$ gives the relationship between the averaged molecular displacement of air and the averaged variation of pressure. As a conclusion of Lu et al.'s model, it is found that the viscous drag forces operating at the fiber surface govern the complex density $\rho(\omega)$ and the thermal forces control the complex bulk modulus $K(\omega)$. As seen in Eqs. (52) and (53), these two quantities is strongly dependent on the term $\rho_0 f/R$, reflecting the inherent dynamic property of sound absorbing process and flow resistance being the fundamental origin of sound absorption.

Generally, in contrast with the facesheet to stiffener interaction and the facesheet to fibrous-material (or air) interaction, the stiffener to fibrous-material (or air) interaction is negligible. It is easy to understand that the direct structural connection between the facesheets and the rib-stiffeners is far stronger than the stiffener to fibrous-material (or air) interaction. As for

the facesheet to fibrous-material interaction, note that the stiffener separations l_x and l_y are generally much larger than the stiffener height d, implying that the contact surface area between the facesheet and fibrous material is much larger than that between the stiffener and fibrous material. Therefore, whilst the vibration of the facesheet is affected significantly by the fibrous material in contact, it has negligible influence on the motion of the short stiffeners. As a result, the fluid-structure coupling here only needs to consider the facesheet to fibrous-material interaction. To ensure the equality of panel velocity and fluid velocity on the panel surface, the momentum equation (i.e., continuity condition of fluid-structure coupling [7,10,35]) is applied:

$$\left[\partial p_{cav}/\partial z\right]_{z=h_1} = \rho_{cav}\omega^2 w_1 , \left[\partial p_{cav}/\partial z\right]_{z=h_1+d} = \rho_{cav}\omega^2 w_2$$
 (54)

where the complex density ρ_{cav} of the fibrous material is related to the complex wavenumber k_{cav} and porosity σ as [12]:

$$\frac{k_{cav}^2}{k_0^2} = \frac{\gamma_s \sigma \rho_{cav}}{\rho_0} \tag{55}$$

Applying the Fourier transform to Eqs. (50) and (54), one obtains:

$$\tilde{p}_{cav}(\alpha,\beta,z) = -\frac{\rho_{cav}\omega^{2}}{\gamma(\alpha,\beta)\left(e^{\gamma d} - e^{-\gamma d}\right)} \begin{cases} \left[\tilde{w}_{1}(\alpha,\beta)e^{\gamma(h_{1}+d)} - \tilde{w}_{2}(\alpha,\beta)e^{\gamma h_{1}}\right]e^{-\gamma z} \\ + \left[\tilde{w}_{1}(\alpha,\beta)e^{-\gamma(h_{1}+d)} - \tilde{w}_{2}(\alpha,\beta)e^{-\gamma h_{1}}\right]e^{\gamma z} \end{cases}$$
(56)

where $\gamma^2 = \alpha^2 + \beta^2 - k_{cav}^2$. More specifically, the pressures acting on the upper and bottom panels are given by:

$$\tilde{p}_{cav}(\alpha, \beta, h_1) = -\frac{\rho_{cav}\omega^2 \left[\tilde{w}_1(\alpha, \beta)\cosh(\gamma d) - \tilde{w}_2(\alpha, \beta)\right]}{\gamma(\alpha, \beta)\sinh(\gamma d)}$$
(57)

$$\tilde{p}_{cav}(\alpha, \beta, h_1 + d) = -\frac{\rho_{cav}\omega^2 \left[\tilde{w}_1(\alpha, \beta) - \tilde{w}_2(\alpha, \beta)\cosh(\gamma d)\right]}{\gamma(\alpha, \beta)\sinh(\gamma d)}$$
(58)

Substituting Eqs. (57) and (58) into Eqs. (36) and (37), respectively, one can rewrite the governing equations as:

$$\left[D_{1}\left(\alpha^{2}+\beta^{2}\right)^{2}-m_{1}\omega^{2}-\frac{\rho_{cav}\omega^{2}\cosh(\gamma d)}{\gamma(\alpha,\beta)\sinh(\gamma d)}\right]\tilde{w}_{1}(\alpha,\beta)+\frac{\rho_{cav}\omega^{2}}{\gamma(\alpha,\beta)\sinh(\gamma d)}\tilde{w}_{2}(\alpha,\beta)$$

$$=\frac{1}{l_{x}}\sum_{m}\left[-R_{Q3}-i\beta^{3}R_{M3}-i\alpha\alpha_{m}\beta R_{T3}\right]\tilde{w}_{1}(\alpha_{m},\beta)+\frac{1}{l_{y}}\sum_{n}\left[-R_{Q1}-i\alpha^{3}R_{M1}-i\alpha\beta\beta_{n}R_{T1}\right]\tilde{w}_{1}(\alpha,\beta_{n})$$

$$+\frac{1}{l_{x}}\sum_{m}\left[R_{Q4}+i\beta^{3}R_{M4}+i\alpha\alpha_{m}\beta R_{T4}\right]\tilde{w}_{2}(\alpha_{m},\beta)+\frac{1}{l_{y}}\sum_{n}\left[R_{Q2}+i\alpha^{3}R_{M2}+i\alpha\beta\beta_{n}R_{T2}\right]\tilde{w}_{2}(\alpha,\beta_{n})$$

$$+\frac{q_{0}}{(2\pi)^{2}}e^{-i(\alpha x_{0}+\beta y_{0})}$$
(59)

$$\left[D_{2}\left(\alpha^{2}+\beta^{2}\right)^{2}-m_{2}\omega^{2}-\frac{\rho_{cav}\omega^{2}\cosh(\gamma d)}{\gamma(\alpha,\beta)\sinh(\gamma d)}\right]\tilde{w}_{2}(\alpha,\beta)+\frac{\rho_{cav}\omega^{2}}{\gamma(\alpha,\beta)\sinh(\gamma d)}\tilde{w}_{1}(\alpha,\beta)$$

$$=-\frac{1}{l_{x}}\sum_{m}\left[-R_{Q4}-i\beta^{3}R_{M4}-i\alpha\alpha_{m}\beta R_{T4}\right]\tilde{w}_{1}(\alpha_{m},\beta)$$

$$-\frac{1}{l_{y}}\sum_{n}\left[-R_{Q2}-i\alpha^{3}R_{M2}-i\alpha\beta\beta_{n}R_{T2}\right]\tilde{w}_{1}(\alpha,\beta_{n})$$

$$-\frac{1}{l_{x}}\sum_{m}\left[R_{Q3}+i\beta^{3}R_{M3}+i\alpha\alpha_{m}\beta R_{T3}\right]\tilde{w}_{2}(\alpha_{m},\beta)$$

$$-\frac{1}{l_{y}}\sum_{n}\left[R_{Q1}+i\alpha^{3}R_{M1}+i\alpha\beta\beta_{n}R_{T1}\right]\tilde{w}_{2}(\alpha,\beta_{n})$$
(60)

To simplify the derivation procedures, the following definitions are introduced:

$$f_1(\alpha,\beta) = (\alpha^2 + \beta^2)^2 - \frac{m_1 \omega^2}{D_1} - \frac{\rho_{cav} \omega^2 \cosh(\gamma d)}{D_1 \gamma(\alpha,\beta) \sinh(\gamma d)}$$
(61)

$$f_2(\alpha,\beta) = (\alpha^2 + \beta^2)^2 - \frac{m_2\omega^2}{D_2} - \frac{\rho_{cav}\omega^2 \cosh(\gamma d)}{D_2\gamma(\alpha,\beta)\sinh(\gamma d)}$$
(62)

As seen in Eqs. (59) and (60), the panel displacements $\tilde{w}_1(\alpha,\beta)$ and $\tilde{w}_2(\alpha,\beta)$ to be solved are not independent but have coupling terms $\tilde{w}_1(\alpha_m,\beta)$, $\tilde{w}_1(\alpha,\beta_n)$, $\tilde{w}_2(\alpha_m,\beta)$ and $\tilde{w}_2(\alpha,\beta_n)$ in the corresponding sum formula. To solve these unknowns, one needs to replace (α,β) by (α_m',β_n') , leading to two sets of simultaneous algebraic equations, as:

$$D_{1}f_{1}(\alpha'_{m},\beta'_{n})\tilde{w}_{1}(\alpha'_{m},\beta'_{n}) + \frac{\rho_{caw}\omega^{2}}{\gamma(\alpha'_{m},\beta'_{n})\sinh[\gamma(\alpha'_{m},\beta'_{n})\cdot d]}\tilde{w}_{2}(\alpha'_{m},\beta'_{n})$$

$$+ \frac{1}{l_{x}} \left[\left(R_{Q3} + i\beta'_{n}^{3}R_{M3} \right) \sum_{m} \tilde{w}_{1}(\alpha_{m},\beta'_{n}) + i\alpha'_{m}\beta'_{n}R_{T3} \sum_{m} \alpha_{m}\tilde{w}_{1}(\alpha_{m},\beta'_{n}) \right]$$

$$+ \frac{1}{l_{y}} \left[\left(R_{Q1} + i\alpha'_{m}^{3}R_{M1} \right) \sum_{n} \tilde{w}_{1}(\alpha'_{m},\beta_{n}) + i\alpha'_{m}\beta'_{n}R_{T1} \sum_{n} \beta_{n}\tilde{w}_{1}(\alpha'_{m},\beta_{n}) \right]$$

$$- \frac{1}{l_{x}} \left[\left(R_{Q4} + i\beta'_{n}^{3}R_{M4} \right) \sum_{m} \tilde{w}_{2}(\alpha_{m},\beta'_{n}) + i\alpha'_{m}\beta'_{n}R_{T4} \sum_{m} \alpha_{m}\tilde{w}_{2}(\alpha_{m},\beta'_{n}) \right]$$

$$- \frac{1}{l_{y}} \left[\left(R_{Q2} + i\alpha'_{m}^{3}R_{M2} \right) \sum_{n} \tilde{w}_{2}(\alpha'_{m},\beta_{n}) + i\alpha'_{m}\beta'_{n}R_{T2} \sum_{n} \beta_{n}\tilde{w}_{2}(\alpha'_{m},\beta_{n}) \right]$$

$$= \frac{q_{0}}{(2\pi)^{2}} e^{-i(\alpha'_{m}x_{0} + \beta'_{n}y_{0})}$$

$$(63)$$

$$\frac{\rho_{cav}\omega^{2}}{\gamma(\alpha'_{m},\beta'_{n})\sinh[\gamma(\alpha'_{m},\beta'_{n})\cdot d]}\tilde{w}_{1}(\alpha'_{m},\beta'_{n}) + D_{2}f_{2}(\alpha'_{m},\beta'_{n})\tilde{w}_{2}(\alpha'_{m},\beta'_{n})
-\frac{1}{l_{x}}\left[\left(R_{Q4} + i\beta'_{n}^{3}R_{M4}\right)\sum_{m}\tilde{w}_{1}(\alpha_{m},\beta'_{n}) + i\alpha'_{m}\beta'_{n}R_{T4}\sum_{m}\alpha_{m}\tilde{w}_{1}(\alpha_{m},\beta'_{n})\right]
-\frac{1}{l_{y}}\left[\left(R_{Q2} + i\alpha'_{m}^{3}R_{M2}\right)\sum_{n}\tilde{w}_{1}(\alpha'_{m},\beta_{n}) + i\alpha'_{m}\beta'_{n}R_{T2}\sum_{n}\beta_{n}\tilde{w}_{1}(\alpha'_{m},\beta_{n})\right]
+\frac{1}{l_{x}}\left[\left(R_{Q3} + i\beta'_{n}^{3}R_{M3}\right)\sum_{m}\tilde{w}_{2}(\alpha_{m},\beta'_{n}) + i\alpha'_{m}\beta'_{n}R_{T3}\sum_{m}\alpha_{m}\tilde{w}_{2}(\alpha_{m},\beta'_{n})\right]
+\frac{1}{l_{y}}\left[\left(R_{Q1} + i\alpha'_{m}^{3}R_{M1}\right)\sum_{n}\tilde{w}_{2}(\alpha'_{m},\beta_{n}) + i\alpha'_{m}\beta'_{n}R_{T1}\sum_{n}\beta_{n}\tilde{w}_{2}(\alpha'_{m},\beta_{n})\right]
= 0$$
(64)

which contain two sets of infinite unknowns: $\tilde{w}_1(\alpha'_m,\beta'_n)$ and $\tilde{w}_2(\alpha'_m,\beta'_n)$, with $m=-\infty$ to $+\infty$ and $n=-\infty$ to $+\infty$. Insofar as the solution converges, these equations can be truncated to retain one set of finite unknowns $\tilde{w}_1(\alpha'_m,\beta'_n)$ and $\tilde{w}_2(\alpha'_m,\beta'_n)$, with $m=-\hat{m}$ to \hat{m} and $n=-\hat{n}$ to \hat{n} (both \hat{m} and \hat{n} are positive integers), and hence can be numerically solved.

2.4 Far field sound radiated pressure

Owing to the fluid-structure interaction of the vibrating panel (bottom panel in the present case) and its surrounding fluid, sound pressure will be radiated from the fluid-structure interface into the far field. Therefore, once the response of the bottom panel $\tilde{w}_2(\alpha,\beta)$ is numerically solved, the radiated sound pressure at the far field can be obtained by employing the established sound radiation theory.

With the origin of the spherical coordinates (r,θ,φ) located at the excitation point (x_0, y_0) , the far field sound pressure $p(r,\theta,\varphi)$ radiated from a vibrating surface with displacement w(x,y) is given by [30]:

$$p(r,\theta,\varphi) = -\rho_0 \omega^2 \frac{e^{ik_0 r}}{2\pi r} e^{i(\alpha x_0 + \beta y_0)} \int_{-\infty}^{+\infty} \int_{-\infty}^{+\infty} w(x,y) e^{-i(\alpha x + \beta y)} dx dy$$
 (65)

where $k_0 = \omega / c_0$, c_0 and ρ_0 are separately the sound speed and air density, and the wavenumbers α and β are:

$$\alpha = k_0 \cos \varphi \sin \theta$$
, $\beta = k_0 \sin \varphi \sin \theta$ (66)

By adopting the Fourier transform of Eq. (35), Eq. (65) becomes:

$$p(r,\theta,\varphi) = -2\pi\rho_0 \omega^2 \left(e^{ik_0 r} / r \right) e^{i(\alpha x_0 + \beta y_0)} \tilde{w}(\alpha,\beta)$$
(67)

For reference, the high frequency asymptote of far field sound pressure radiated by an *unstiffened* plate [3] is introduced, as:

$$p_{asy} = \rho_0 q_0 e^{ik_0 r} / 2\pi mr \tag{68}$$

The far field sound pressure radiated by the present orthogonally rib-stiffened sandwich structure with cavity absorption is then given in the form of sound pressure level (SPL) in decibel scales (dB) with respect to p_{gsy} , as:

$$SPL = 10 \cdot \log_{10} \left(p/p_{asy} \right)^2 \tag{69}$$

3. Numerical results and discussions

In this section, representative examples for the on-axis (i.e., on the axis $\theta=\varphi=0$) far field pressure is numerically calculated to explore the sound radiation characteristics of infinite orthogonally rib-stiffened sandwich structures with fibrous material filled cavity. Note that, on the selected axis (i.e., $\theta=\varphi=0$), the stationary phase wavenumbers $\bar{\alpha}$ and $\bar{\beta}$ are both equal to zero.

The material properties and structural dimensions of the sandwich structure are taken as follows. Both the face panels and rib-stiffeners are made of aluminum, with Young's modulus $E=70\,\mathrm{GPa}$, density $\rho=2700\,\mathrm{kg/m^3}$, Poisson ratio $\nu=0.33$, and loss factor $\eta_1=\eta_2=0.01$. The thickness of the two face panel are $h_1=h_2=2\,\mathrm{mm}$, and that of rib-stiffeners are $t_x=t_y=1\,\mathrm{mm}$. The depth of air cavity (i.e., height of rib connections; see Fig. 1) is $d=0.025\,\mathrm{m}$. For air at normal temperature and atmospheric pressure, it is assumed that $\rho_0=1.21\,\mathrm{kg/m^3}$, $N_\mathrm{pr}=0.702$, $\gamma_s=1.4$, $P_0=101320\,\mathrm{N/m^2}$ and $c_0=343\,\mathrm{m/s}$. Fiberglass is selected as the cavity filling material, with porosity $\sigma=0.95$ and flow resistivity $R=24000\,\mathrm{Nm/s^4}$. The time-harmonic point force with unit amplitude acts on the upper panel at location $(l_x/2, l_y/2)$. With these system parameters, the present theoretical model is used to examine the influence of fiberglass material in the cavity (partitioned by the lattice core) on the sound radiation characteristics of the sandwich structure. For comparison, the sound radiation behaviors of sandwich structures with pure air cavity (i.e., air-structure coupling effect included) and vacuum cavity (i.e., fluid-structure coupling effect ignored) are also considered.

3.1 Convergence check for numerical solution

As previously mentioned, the infinite simultaneous algebraic equations are truncated so that one only needs to solve a finite system of equations containing a finite number of unknowns. More specifically, only $M = 2\hat{m} + 1$ and $N = 2\hat{n} + 1$ unknowns are retained, associated separately with subscripts m and n, leading to the same number of harmonic wave components in the x - and y -directions. Insofar as a sufficiently large number of terms are retained, the finite system is capable of ensuring the convergence and accuracy of the solution. The well acknowledged criterion [1,15] is employed, which assumes that once the solution converges at a given frequency, it converges for all lower frequencies. Therefore, the required number of unknowns is determined by the highest frequency of interest (10 kHz in the present study). To check the convergence of the solution, a numerical test is carried out by calculating the SPL at 10 kHz, with increasingly more terms used in Eqs. (63) and (64), as shown in Fig. 3. It can be seen from Fig. 3 that, when \hat{m} and \hat{n} both have a value of 10, solution convergence is ensured at 10 kHz. Consequently, following the

above mentioned criterion, the values of \hat{m} and \hat{n} are both taken as 10 (i.e., retaining 441 unknowns in the finite system) for all frequencies below 10kHz, which is sufficient to ensure the convergence and accuracy of the solution.

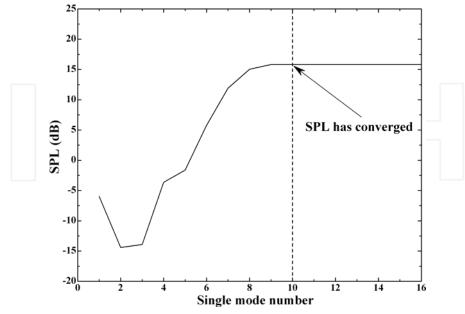


Fig. 3. Convergence check of numerical solution for sound radiation of an infinite orthogonally rib-stiffened sandwich structure with stiffener separations (l_x , l_y) = (0.20m, 0.20m) when excited by a harmonic point force at 10 kHz

3.2 Validation of theoretical modeling

To check the validity of the proposed model, the model (simplified version) is used to calculate the sound pressure level radiated from an orthogonally rib-stiffened single panel and the predictions are compared in Fig. 4 with those obtained by Mace [3]. To degrade the present model for sandwich structures to cover rib-stiffened single panels, negligibly small values are assigned to the prime parameters (i.e., Yong's modulus E, density ρ and thickness h) of one face panel of the sandwich whilst the remaining system parameters are identical to those used by Mace [3].

It can be seen from Fig. 4 that overall the present predictions agree excellently well with those of Mace: only slight deviations exist beyond 5000 Hz. These discrepancies in the high frequency range are expected, which can be attributed to the difference in vibration modeling of the rib-stiffeners between the present model and Mace's theory. The rib-stiffeners were modeled as Euler beams in Mace's theory [3], meaning that only the bending moments and the inertial effect of the tensional forces of the rib-stiffeners are considered. In contrast, the present model accounts for all possible motions of the rib-stiffeners, including tensional forces, bending and torsional moments as well as their inertial effects. Therefore, insofar as the dynamic responses and sound radiation of rib-stiffened plates are of concern,

the present model provides a more precise theoretical tool than the beam-based theory of Mace. The discrepancies between the two theories in the high frequency range of Fig. 4 just demonstrate the necessity of accurately modeling the motion of the rib-stiffeners.

To further check the accuracy of the present model for the double-panel case, the model is degraded to reproduce Takahashi's results [11] for rib-stiffened double-panel structures, as shown in Fig. 5. The relevant geometrical dimensions and material property parameters are identical as those of Takahashi. Again, the model predictions fit well with Takahashi's theoretical results, with only slight divergences appearing at relatively high frequencies. These divergences are attributed to the additional consideration of inertial effects corresponding to the bending moments and torsional moments in the present model, which Takahashi did not take into account.

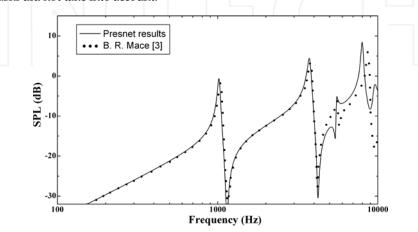


Fig. 4. Comparison between present model predictions and those by Mace [3] for orthogonally rib-stiffened single panel excited by time-harmonic point force at location (0, 0)

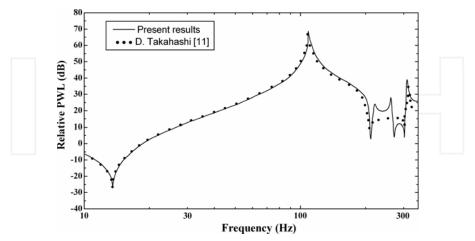


Fig. 5. Comparison between model predictions and theoretical results of Takahashi [11] for ribstiffened double-panel structure excited by time-harmonic point force at location $(l_x/2, l_y/2)$

To a large extent, the comparisons made above may be regarded as acceptable validations for the proposed theoretical model, because all the theoretical formulations have been involved in the numerical calculation. In particular, if a theoretical model can be degraded to obtain the same results for simplified cases, its accuracy and feasibility would be better than the case when it can only give results similar to those obtained with its counterpart models.

3.3 Influence of air-structure coupling effect

Together with the equivalent fluid model for fibrous sound absorptive materials, the present model is able to characterize the sound radiation characteristics of lightweight lattice-cored sandwich structures filled with fibrous materials, such as fiberglass considered here. Note also that the model can be degraded to describe sandwich structures with either air cavity (i.e., air-structure coupling effect included) or vacuum cavity (i.e., fluid-structure coupling effect ignored). Therefore, comparisons amongst the three different kinds of sandwiches under time-harmonic point force excitation can be performed to assess the influences of air-structure coupling effect and fibrous filling material on sound radiation.

To better evaluate the influences of air-structure coupling effect and fibrous material, the location of point force acting on the face panel is selected at the center of one lattice cell, i.e., $(l_x/2, l_y/2)$, away from the conjunction between the face panel and rib-stiffeners. The predicted sound pressure level (SPL) radiated by the three different sandwich structures is plotted in Figs. 6, 7, and 8 as a function of frequency for (l_x, l_y) = (0.20m, 0.20m), (0.35m, 0.35m) and (0.50m, 0.50m), respectively. For each pair of stiffener spacing selected, three kinds of sandwich configurations are compared: (i) vacuum cavity; (ii) air cavity; (iii) cavity filled with fiberglass.

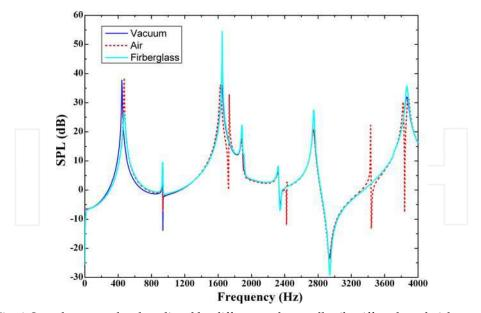


Fig. 6. Sound pressure levels radiated by different orthogonally rib-stiffened sandwich structures plotted as functions of frequency for stiffener separations (l_x , l_y) = (0.20m, 0.20m)

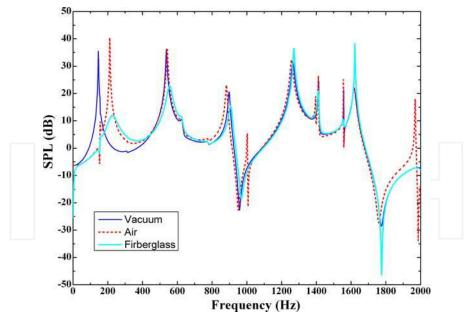


Fig. 7. Sound pressure levels radiated by different orthogonally rib-stiffened sandwich structures plotted as functions of frequency for stiffener separations (l_x =0.35m, l_y =0.35m)

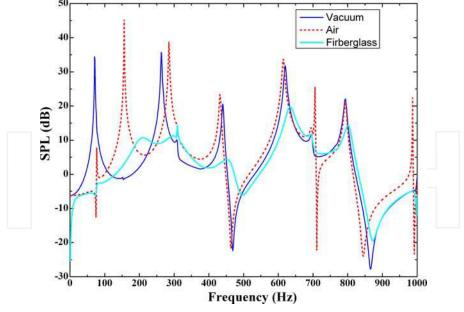


Fig. 8. Sound pressure levels radiated by different orthogonally rib-stiffened sandwich structures plotted as functions of frequency for stiffener separations (l_x =0.50m, l_y =0.50m)

At first glance, it can be seen from Figs. 6-8 that the air cavity case shows several additional peaks and dips on the SPL versus frequency curve. This is caused by air cavity interacting with the face panels through air-structure coupling. Besides these additional peaks and dips, it is also observed that the air-structure coupling effect plays an increasingly significant role in structure sound radiation with increasing rib-stiffener separation. This is reflected by the enlarged deviations between the two curves associated separately with the vacuum case and the air cavity case as the rib-stiffener separation is increased. In particular, when the separation is relatively large, air-structure coupling exerts a visible effect on the location of maximum sound radiation especially in low frequency range. The air-structure coupling is in effect by means of pumping effect, that is, the air cavity partitioned by the face panels and rib-stiffeners has timely changing pressure as its volume alters with the dynamic displacements of these two face panels, often imposing a converse force on the panels. In the case of rib-stiffener separation being relatively large, a considerable area of the panels is exposed to the impinging of air cavity pressure. It is thence understandable that the air-structure coupling effect may not be ignored when the rib-stiffeners are sparsely distributed.

3.4 Influence of fibrous sound absorptive filling material

In contrast to the air cavity case, the fiberglass case exhibits almost the same trends as the vacuum one, especially when the stiffener separation is relatively small, although the discrepancies between the two cases increase as the stiffener separation is increased. Note that the air-structure coupling effect is not present in the vacuum case whilst it is eliminated in the fiberglass case (the presence of fiberglass in the cavity significantly changes the behavior of the cavity). This is also the reason why the fiberglass case exhibits almost the same trend as the vacuum one: the discrepancies between the two cases enlarging with increasing stiffener separation actually reflect the combined effect of fiberglass stiffness and damping on structure responses.

It is understandable that the stiffness of the cavity-filling fiberglass reinforces the structural connection between the two face panels, enabling more vibration energies transmitted from the upper panel to the bottom one and thus causing larger sound radiation pressure levels. Conversely, fiberglass can dissipate acoustic energy via viscous drag forces and thermal exchange between the air and fibers, and hence decreases sound radiation. In addition, both the stiffness and damping of the fiberglass material are frequency dependent [17,19,22]. Consequently, the fact that the discrepancies between the vacuum and fiberglass cases increase with increasing stiffener separation can be well explained.

The periodically distributed rib-stiffeners with relatively narrow separations restrict the deformation of fiberglass in-between, offering therefore the fiberglass a larger stiffness than that inserted between those stiffeners having wider separations. That the fiberglass case exhibits the same trend as the vacuum one when the separation is small (e.g., l_x = 0.20 m and l_y = 0.20 m, as shown in Fig. 6) may be attributed to the balance of the converse effects of fiberglass stiffness and damping on sound radiation. More specifically, whilst damping is dominant at low frequencies, causing decreased sound radiation in the first peak, stiffness dominates at high frequencies, resulting in increased sound radiation in the following peaks (Figs. 7 and 8). As mentioned above, the stiffness of fiberglass decreases with increasing stiffener separation. Therefore, as the separation is increased, the frequency range dominated by stiffness (i.e., stiffness-controlled region) is shifted to higher frequencies and

that dominated by damping (i.e., damping-controlled region) is widened. Correspondingly, in Fig. 7 the first three sound radiation peaks of the fiberglass case are lower than those of the vacuum one, and all the sound radiation peaks of the fiberglass case are significantly lower than those of the vacuum one in Fig. 8.

It may thence be deduced that the fiberglass-filled cavity affects structural radiation through the combined effects of fiberglass stiffness and damping (both being frequency dependent), the balance of which is significantly influenced by stiffener separation. It is therefore possible to optimize the stiffener separation and fiberglass porosity (both indirectly related to the stiffness and damping of fiberglass) to reduce structure sound radiation to an acceptable level required in specific cases.

4. Conclusions

The sound radiation characteristics of an infinite orthogonally rib-stiffened sandwich structure having cavity-filling fibrous sound absorptive material have been formulated by a comprehensive theoretical model when the structure is excited by a time-harmonic point force. The novelty of this work is to provide a general theoretical framework to address sound radiation issues of sandwich structures filled with fibrous sound absorptive materials, which can be degraded to deal with relatively simple structures. In the theoretical model, the vibration behaviors of the rib-stiffeners are accounted for by including all possible forces and moments exerted on the face panels by the rib-stiffeners in the governing equations. The propagation of sound in the fibrous material is modeled by adopting an equivalent fluid model with frequency dependent dynamic density and bulk modulus, with viscous drag force and thermal exchanges between air and fibers taken into account. The technique of Fourier transform is applied to solve the governing equations, resulting in an infinite set of simultaneous algebraic equations, which can be truncated and numerically solved.

Numerical calculations are subsequently carried out to explore the influences of air-structure coupling effect and fibrous sound absorptive materials on structure sound radiation. The model is validated by comparing the present model predictions with previously published data, with excellent agreement achieved especially at low frequencies. Nevertheless, slight deviations emerge at high frequencies, which just demonstrate the superiority of the present model.

Special attention is then focused on the effects of air-structure coupling and fibrous sound absorptive materials on sound penetration. This is explored by comparing three different sandwich structures: partitioned cavity in vacuum, filled with air, and filled with fiberglass. Interesting physical features emerging from the comparison are well interpreted by considering the combined effects of fiberglass stiffness and damping as well as the influence of rib-stiffener separation. It is found that the air-structure coupling effect induces additional peaks and dips in the SPL versus frequency curves, which plays an increasingly significant effect on structure sound radiation as the stiffener separation is increased. In particular, it is concluded that the fiberglass-filled cavity exerts its impact on wave penetration (finally on structural radiation) through the combined effects of fiberglass stiffness and damping (both frequency dependent), the balance of which is significantly affected by stiffener separation. This may provide a convenient and efficient tool to optimize

the porosity, cell size and other topological parameters of fiberglass (indirectly altering its stiffness and damping) in conjunction with stiffener separation to reduce the structure vibration and sound radiation to an acceptable level required in specific situations.

As a future research forecast, the theoretical model for sandwich composite structures considered here (i.e., square lattice-cored sandwich structures filled with fibrous materials) can be further extended to study the acoustical performance of sandwich composite structures having laminated composites as skins, since these structures have been increasingly applied in aerospace and astronautic fields.

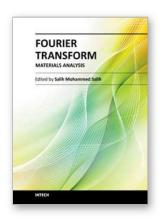
5. Acknowledgements

This work is supported by the National Basic Research Program of China (2011CB6103005), the National Natural Science Foundation of China (11072188, 11102148, 10825210 and 11021202) and the Fundamental Research Funds for the Central Universities.

6. References

- [1] Xin FX, Lu TJ, Chen CQ. Sound transmission through simply supported finite doublepanel partitions with enclosed air cavity. ASME J Vib Acoust 2010;132(1):011008: 1-11.
- [2] Mace BR. Sound radiation from a plate reinforced by two sets of parallel stiffeners. J Sound Vib 1980;71(3):435-441.
- [3] Mace BR. Sound radiation from fluid loaded orthogonally stiffened plates. J Sound Vib 1981;79(3):439-452.
- [4] Yin XW, Gu XJ, Cui HF, Shen RY. Acoustic radiation from a laminated composite plate reinforced by doubly periodic parallel stiffeners. J Sound Vib 2007;306(3-5):877-889.
- [5] Xin FX, Lu TJ, Chen CQ. Dynamic response and acoustic radiation of double-leaf metallic panel partition under sound excitation. Comput Mater Sci 2009;46(3):728–732.
- [6] Maury C, Gardonio P, Elliott SJ. Active control of the flow-induced noise transmitted through a panel. AIAA J. 2001;39(10):1860-1867.
- [7] Xin FX, Lu TJ, Chen CQ. External mean flow influence on noise transmission through double-leaf aeroelastic plates. AIAA J. 2009;47(8):1939-1951.
- [8] Xin FX, Lu TJ. Analytical and experimental investigation on transmission loss of clamped double panels: Implication of boundary effects. J Acoust Soc Am 2009;125(3):1506-1517.
- [9] Xin FX, Lu TJ, Chen CQ. Vibroacoustic behavior of clamp mounted double-panel partition with enclosure air cavity. J Acoust Soc Am 2008;124(6):3604-3612.
- [10] Lin G-F, Garrelick JM. Sound transmission through periodically framed parallel plates. J Acoust Soc Am 1977;61(4):1014-1018.
- [11] Takahashi D. Sound radiation from periodically connected double-plate structures. J Sound Vib 1983;90(4):541-557.
- [12] Trochidis A, Kalaroutis A. Sound transmission through double partitions with cavity absorption. J Sound Vib 1986;107(2):321-327.
- [13] Alba J, Ramis J, Sanchez-Morcillo VJ. Improvement of the prediction of transmission loss of double partitions with cavity absorption by minimization techniques. J Sound Vib 2004;273(4-5):793-804.

- [14] Mead DJ, Pujara KK. Space-harmonic analysis of periodically supported beams: response to convected random loading. J Sound Vib 1971;14(4):525-532.
- [15] Lee JH, Kim J. Analysis of sound transmission through periodically stiffened panels by space-harmonic expansion method. J Sound Vib 2002;251(2):349-366.
- [16] Wang J, Lu TJ, Woodhouse J, Langley RS et al. Sound transmission through lightweight double-leaf partitions: Theoretical modelling. J Sound Vib 2005;286(4-5):817-847.
- [17] Legault J, Atalla N. Numerical and experimental investigation of the effect of structural links on the sound transmission of a lightweight double panel structure. J Sound Vib 2009;324(3-5):712-732.
- [18] Xin FX, Lu TJ. Analytical modeling of fluid loaded orthogonally rib-stiffened sandwich structures: Sound transmission. J Mech Phys Solids 2010;58(9):1374-1396.
- [19] Panneton R, Atalla N. Numerical prediction of sound transmission through finite multilayer systems with poroelastic materials. J Acoust Soc Am 1996;100(1):346-354.
- [20] Sgard FC, Atalla N, Nicolas J. A numerical model for the low frequency diffuse field sound transmission loss of double-wall sound barriers with elastic porous linings. J Acoust Soc Am 2000;108(6):2865-2872.
- [21] Brown SM, Niedzielski J, Spalding GR. Effect of sound-absorptive facings on partition airborne-sound transmission loss. J Acoust Soc Am 1978;63(6):1851-1856.
- [22] Allard J-F, Champoux Y. New empirical equations for sound propagation in rigid frame fibrous materials. J Acoust Soc Am 1992;91(6):3346-3353.
- [23] Rumerman ML. Vibration and wave propagation in ribbed plates. J Acoust Soc Am 1975;57(2):370-373.
- [24] Lu TJ, Hess A, Ashby MF. Sound absorption in metallic foams. J Appl Phys 1999;85(11):7528-7539.
- [25] Wang XL, Lu TJ. Optimized acoustic properties of cellular solids. J Acoust Soc Am 1999;106(2):756-765.
- [26] Lu TJ, Chen F, He D. Sound absorption of cellular metals with semiopen cells. J Acoust Soc Am 2000;108(4):1697-1709.
- [27] Lu TJ, Kepets M, Dowling A. Acoustic properties of sintered FeCrAlY foams with open cells (I): Static flow resistance. Sci China Ser E: Tech Sci 2008;51(11):1803-1811.
- [28] Lu TJ, Kepets M, Dowling A. Acoustic properties of sintered FeCrAlY foams with open cells (II): Sound attenuation. Sci China Ser E: Tech Sci 2008;51(11):1812-1837.
- [29] Zwikker C, Kosten CW, 1949, Sound absorbing materials, Elsevier, New York.
- [30] Morse PM, Ingard KU, 1968, Theoretical acoustics, McGraw-Hill, New York.
- [31] Biot MA. Theory of propagation of elastic waves in a fluid-saturated porous solid. I. Low-frequency range. J Acoust Soc Am 1956;28(2):168-178.
- [32] Biot MA. Theory of propagation of elastic waves in a fluid-saturated porous solid. II. Higher frequency range. J Acoust Soc Am 1956;28(2):179-191.
- [33] Johnson DL, Koplik J, Dashen R. Theory of Dynamic Permeability and Tortuosity in Fluid-Saturated Porous-Media. J. Fluid Mech. 1987;176(379-402.
- [34] Xin FX, Lu TJ. Sound radiation of orthogonally rib-stiffened sandwich structures with cavity absorption. Compos Sci Technol 2010;70(15):2198-2206.
- [35] Xin FX, Lu TJ. Analytical modeling of sound transmission across finite aeroelastic panels in convected fluids. J Acoust Soc Am 2010;128(3):1097-1107.



Fourier Transform - Materials Analysis

Edited by Dr Salih Salih

ISBN 978-953-51-0594-7 Hard cover, 260 pages Publisher InTech Published online 23, May, 2012 Published in print edition May, 2012

The field of material analysis has seen explosive growth during the past decades. Almost all the textbooks on materials analysis have a section devoted to the Fourier transform theory. For this reason, the book focuses on the material analysis based on Fourier transform theory. The book chapters are related to FTIR and the other methods used for analyzing different types of materials. It is hoped that this book will provide the background, reference and incentive to encourage further research and results in this area as well as provide tools for practical applications. It provides an applications-oriented approach to materials analysis written primarily for physicist, Chemists, Agriculturalists, Electrical Engineers, Mechanical Engineers, Signal Processing Engineers, and the Academic Researchers and for the Graduate Students who will also find it useful as a reference for their research activities.

How to reference

In order to correctly reference this scholarly work, feel free to copy and paste the following:

F. X. Xin and T. J. Lu (2012). Fourier Transform Sound Radiation, Fourier Transform - Materials Analysis, Dr Salih Salih (Ed.), ISBN: 978-953-51-0594-7, InTech, Available from: http://www.intechopen.com/books/fourier-transform-materials-analysis/fourier-transform-sound-radiation



InTech Europe

University Campus STeP Ri Slavka Krautzeka 83/A 51000 Rijeka, Croatia Phone: +385 (51) 770 447

Fax: +385 (51) 686 166 www.intechopen.com

InTech China

Unit 405, Office Block, Hotel Equatorial Shanghai No.65, Yan An Road (West), Shanghai, 200040, China 中国上海市延安西路65号上海国际贵都大饭店办公楼405单元

Phone: +86-21-62489820 Fax: +86-21-62489821